Three-magnon splitting and confluence processes for spin-wave excitations in yttrium iron garnet films: Wave vector selective Brillouin light scattering measurements and analysis

César L. Ordóñez-Romero,[1,2] Boris A. Kalinikos,[1,3] Pavol Krivosik,[1,4] Wei Tong,[1] Pavel Kabos,[5] and Carl E. Patton[1]
[1]*Department of Physics, Colorado State University, Fort Collins, Colorado 80523, USA*
[2]*Universidad Nacional Autónoma de México, Ciudad Universitaria, México D.F., Mexico*
[3]*St. Petersburg Electrotechnical University, 197376 St. Petersburg, Russia*
[4]*Slovak University of Technology, 81219 Bratislava, Slovak Republic*
[5]*National Institute of Standards and Technology, Boulder, Colorado 80305, USA*
(Received 5 February 2009; published 27 April 2009)

Brillouin light scattering (BLS) has been used to observe and confirm the existence of nonlinear three magnon splitting and confluence processes for propagating spin waves in the magnetostatic backward volume wave configuration. Wave vector and frequency selective BLS techniques were also used to provide a quantitative map of the wave vector make-up for the parametrically excited half-frequency dipole-exchange spin wave (DESW) split magnons and the confluence magnons that result from the recombination of these DESW modes. The experimental wave vector maps for the product splitting and confluence magnons matched nicely with those expected from spin-wave theory. The data were obtained with (1) a strip line excitation/detection transducer structure, (2) forward-scattering BLS optics, (3) a fixed magnetic field of 352 Oe applied along the propagation direction, (4) pumping frequencies from 2.5 down to 2.1 GHz, (5) and cw input powers from 200 μW to 6 mW. The wave vector selective measurements utilized variable diameter circular diaphragms, rotatable slit apertures, and circular light blocks to access spin waves with wave numbers from about 100 to 3.6×10^4 rad/cm and the full 360° range of propagation angles.

DOI: 10.1103/PhysRevB.79.144428 PACS number(s): 75.30.Ds, 05.45.−a, 78.35.+c, 85.70.Ge

I. INTRODUCTION

During the last several decades, extremely low loss magnetic thin films, and yttrium iron garnet (YIG) films in particular, have been used to study a wide variety of linear and nonlinear spin-wave phenomena at microwave frequencies. In addition to the relevance of these effects to problems in magnetodynamics, the results are also of fundamental importance for the understanding of wave behavior in dispersive dissipative media in general. Currently there are three main areas of interest in the study of nonlinear magnetization dynamics in magnetic films, (i) microwave-driven parametric spin-wave processes, often termed Suhl instabilities,[1–3] (ii) modulational instability and stationary spin-wave excitations such as envelope solitons,[4–8] and (iii) chaotic nonlinear dynamics.[9,10] All three of these classes of nonlinear magnetodynamics effects involve nonlinear spin-wave interactions through so-called three or four wave processes.

This paper focuses on item (i), and in particular, three wave splitting and confluence processes and the elucidation of these interactions by wave vector selective Brillouin light scattering (BLS). In 2000, Synogach *et al.*[1] were the first to demonstrate the role of parametric three wave processes in the creation of ultrashort microwave pulses in YIG film spin-wave propagation structures. The data, while convincing, were comprised of microwave results only. In 2003, Mathieu *et al.*[2] were able to use time and space resolved BLS techniques to obtain direct images of the propagating half-frequency spin waves produced by the three wave splitting interactions. Interestingly, these images revealed very low velocity wedge shaped wave fronts with the parametric spin waves concentrated along the leading edge. These results had one missing link, namely, no direct evidence for the companion confluence process by which the half-frequency magnons recombine to make the narrow pulse magnons at the initial signal frequency.

This missing link is addressed here. Continuous wave microwaves were used to excite spin waves in a YIG film magnetostatic backward volume wave (MSBVW) propagation structure. Precision BLS spectra for different input power levels revealed both the half-frequency peak that is the signature of the parametric magnons from the three wave splitting as well as a prominent signal that was only slightly downshifted in frequency from the initial pumping frequency. Detailed wave vector selective BLS measurements served to identify this signal as due to a confluence of the parametric magnons. This is the first direct observation of three wave confluence processes in magnetic systems. It also represents the first direct observation of splitting for MSBVW spin waves.

Section II describes the basic BLS/microwave experiment as well as operational details on wave vector selective measurements. Section III presents representative BLS data that comprise the experimental evidence for the three wave splitting and confluence processes and makes qualitative connections with the governing dipole-exchange spin wave (DESW) frequency wave number dispersion relations. Section IV presents additional wave vector selective BLS data that serve to identify the explicit nature of the splitting and confluence magnon products from the pumped MSBVW spin waves. Section V provides brief comments on the effect of small changes in the pumping frequency on the magnon splitting and confluence processes elucidated in the earlier sections. Section VI provides a summary and conclusions.

II. MICROWAVE AND BRILLOUIN LIGHT SCATTERING SETUP

The key microwave component of the setup was the spin-wave propagation structure. This was comprised of a long and narrow YIG film strip in a standard MSBVW spin-wave (SW) delay line configuration.[7] The strip was 20 mm long, 2 mm wide, and 6.3 μm thick. The low loss YIG film was grown by standard liquid phase epitaxy techniques. The 5 GHz ferromagnetic resonance half-power line width was about 0.5 Oe. A pair of 50 μm-wide and 2 mm-long microstrip transducers with a separation of 7 mm was used to excite and detect the propagating spin waves. For propagation in the MSBVW configuration, the static external field H was applied parallel to the long dimension of the strip and the SW propagation direction. The field was set at a nominal value of 352 Oe for all of the measurements. The cw microwave input was at a pumping frequency f_p of 2.5 GHz for most of the measurements. For the frequency effect study in Sec. V, additional f_p values from 2.4 to 2.1 GHz were also used. For the BLS measurements shown below, the nominal input microwave power level at the launch transducer ranged from about 200 μW to 6 mW. Some of the preliminary microwave measurements were done at powers down to 1 μW or so. These data indicated a Suhl threshold power level in the range of 1 μW or so.

The above field-frequency operating point was chosen subject to two criteria. The first is the realization of a strong SW signal at the output transducer. 2.5 GHz sits at the maximum of the MSBVW amplitude vs frequency transmission curve for the structure at 352 Oe. This operating point corresponded to a wave number k for the pumped magnons on the lowest-order branch MSBVW dipole-exchange spin wave of about 100 rad/cm. The second is the need to ensure that three wave splitting processes are allowed. In practical terms, this means that spin waves at $f_p/2$ are supported by the propagation structure.[2] At $H=352$ Oe, the bottom of the MSBVW dipole-exchange spin-wave band sits at about 1.1 GHz, well below $f_p/2$.

The BLS measurements were performed using a multipass tandem Fabry-Pérot (TFP) interferometer in a forward-scattering configuration, with and without wave vector selectivity. The basic forward-scattering approach to the analysis of pumped spin-wave excitations in YIG films was first developed by Srinivasan and co-workers.[11,12] Wave vector selective BLS analysis techniques for spin waves were first developed by Wilber and co-workers.[13–15]

The overall measurement approach used here follows Mathieu *et al.*[2] For the current experiments, a 514.5 nm wavelength linearly polarized argon-ion laser light was focused onto the YIG film by a 12 cm focal length lens at normal incidence with 10 mW incident power. The directly transmitted and scattered light was collected by a 50 mm focal length, and 30 mm diameter F1.4 camera lens. A polarizing filter set perpendicular to the incident light polarization was used to reduce substantially the intensity of the directly transmitted beam. Magnon scattered light generally experiences a 90° rotation in polarization from the incident beam.

The wave vector selective BLS measurements were done in two ways. First, different sized on-axis circular apertures formed from a variable diaphragm behind the collection lens were used to vary the maximum magnon wave number k_{max} for the forward scattered light. Second, wave vector directions were selected though the use of a 1 mm wide slit-type aperture placed behind the collection lens. The slit orientation relative to the applied field defines the usual polar spin-wave propagation angle θ_k.

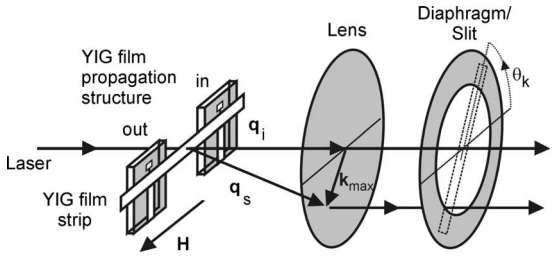

FIG. 1. Schematic diagram of the wave vector selection scattering geometry. The laser light is incident on the yttrium iron garnet film spin-wave propagation structure at wave vector $\mathbf{q}_i$, with a scattered light wave vector $\mathbf{q}_s$ and a magnon wave vector $\mathbf{k}_{max}$ oriented at an angle θ_{max} relative to the direction of the applied field **H**. The collection lens and the diaphragm slit assembly define the selected magnon wave vector.

Figure 1 illustrates the scattering geometry and the wave vector selection process described above. The figure shows the YIG film propagation structure and the collection optics. The arrows show the incident light with wave vector $\mathbf{q}_i$ and the scattered light at $\mathbf{q}_s$ that results from the interaction with a magnon with wave vector $\mathbf{k}_{max}$. This upper limit on $|\mathbf{k}_{max}|$ is defined by the radius of the on-axis diaphragm shown schematically on the far right side of the diagram. The opening limits the scattered light into the spectrometer to those photons that derive from magnons with wave numbers (k) less than some k_{max}. If one uses the 1 mm wide slit instead of the diaphragm, as indicated by the dashed lines, then one can further limit the selected magnon wave vector to a specific propagation angle θ_k. This is strictly true for k values above 1000 rad/cm or so, well within the bounds of the data considered below. A full slit that extends over the entire aperture of the collection lens, as indicated by the dashed rectangle, was used for the initial scans to determine the θ_k values for strong scattering. A special slit that extends only in one direction from the optic axis was used for the quantitative wave vector selective measurements to be considered in Sec. IV.

For the wave-number measurements for the confluence magnons in Sec. IV, an additional wave vector selection process was used. In this set up, instead of a diaphragm, different size on-axis circular light blocks were used. The diameter of the block plays the same role as the diameter of the diaphragm in Fig. 1, except than one now selects out wave numbers above some k_{min} value instead of k values below some k_{max}.

Through the above scheme, one can perform a full range of wave vector selective BLS measurements. Separate data runs for different diameter (d) diaphragms or circular light blocks, for example, can allow one to separate out the scattering associated with specific wave numbers. Diaphragms with d values from 1 to 30 mm were used, typically in in-

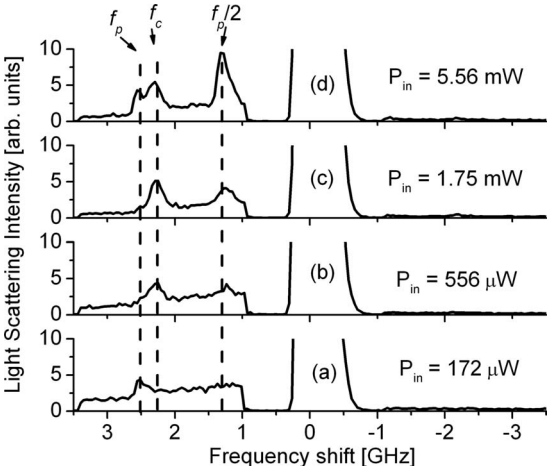

FIG. 2. Representative Brillouin light scattering spectra of scattering intensity vs frequency for different input microwave cw power levels (P_{in}), as indicated. The pump frequency (f_p) was 2.5 GHz. The static external field was set to 352 Oe. The nominal spectrometer free spectral range was 8 GHz. There were no wave vector selective diaphragms in place and the measuring time was the same for all scans. The vertical dashed lines and labels identify different peaks in the spectra at f_p, at f_c, slightly below f_p, and at $f_p/2$.

crements of 1 or 2 mm. The corresponding k_{max} values are 1.2×10^3 rad/cm and 3.6×10^4 rad/cm, respectively. Light blocks with d values from 2 to 10 mm were used. These diameters give a range of k_{max} from 2.4×10^3 to 1.2×10^4 rad/cm. Measurements were always made with the same light intensity and measuring time. Once the wave number has been determined, data obtained with a slit aperture can be used to separate out the product magnons as a function of propagation angle. The wave vector selectivity capability is crucial to the identification of the product spin waves for the nonlinear three magnon splitting and confluence processes that are the focus of this paper. The data presented in Sec. IV will illustrate the very different wave vector makeup for the parametrically excited DESW $f_p/2$ magnons from the splitting process and the product spin waves that come from the confluence of these magnons.

III. PARAMETRIC DESW AND CONFLUENCE MAGNONS

How do the BLS data reveal the presence of the relevant magnons? Figure 2 shows representative BLS spectra of scattering intensity vs frequency for different input cw power levels, as indicated. The frequency axis shows the scattered photon frequency relative to the laser frequency. The frequency axis goes from positive, or anti-Stokes (AS), on the left, to negative, or Stokes (S), on the right. The strong Rayleigh peak at zero frequency comes from the laser line. The incident beam was positioned in the middle of the YIG strip about 2 mm down line from the input transducer. The microwave pumping frequency was 2.5 GHz. The static magnetic field was set at 352 Oe. All measurements were made with the same incident light intensity, the wave vector selective diaphragm removed, and the same TFP scanning parameters.

Note also that the scans in Fig. 2 show magnon signals only on the positive frequency AS side of the spectra. This AS region was scanned at a slow scan rate in order to bring out the magnon structure. Note that this AS region corresponds to scattering in which one of the microwave or parametrically pumped magnon is destroyed and a photon is created. Generally speaking, the BLS peaks for the pumped magnons at f_p and the $f_p/2$ split magnons are found to be stronger on the AS side of the spectra. Intuitively, this is consistent with the nature of the scattering from magnons driven to large occupation numbers by either the microwave pumping process or the subsequent interactions that produce the parametric magnons. For the confluence magnons, however, it turns out that the Stokes as well the Anti-Stokes sides of the spectra are needed to obtain a full picture of the excited modes. Such AS-S confluence magnon effects will be considered in Sec. IV.

The spectra examples in Fig. 2. show three things. (1) There is a peak in the spectra at the pumping frequency that is strong at low power, weakens at intermediate power levels, and then strengthens again at the highest power shown. (2) As the power is increased, one sees an additional peak at $f_p/2\approx1.25$ GHz appear and grow in strength. (3) One can also see the appearance and growth of a third peak at $f_c\approx2.25$ GHz, positioned slightly below the f_p peak in frequency, as the power level is increased.

In reference to item (1), the initial drop and subsequent increase in intensity for the peak in the spectra as the power level is increased is a likely indication of the role of the three magnon processes that are in play here. Microwave data for manganese ferrite (Mg-F) in the initial Suhl paper on ferromagnetic resonance saturation shows a gradual decrease in the microwave loss as one moves above threshold.[3] The data in Ref. 3, however, do not extend to the extreme 25–40 dB above threshold levels needed to match the results in Fig. 2. Moreover, the nature of the Mg-F samples is not specified. One possible scenario in the present context is that, more and more of the energy of the pumped magnons is passed to the parametric magnons and the peak at f_p drops in strength as the power is initially increased well above threshold. As the power is increased further, these parametric processes level off and the f_p peak grows again.

For item (2), the growth of the $f_p/2$ magnon splitting peak with increasing power provides direct evidence for the scenario above. This is actually a threshold effect similar to that found for Suhl processes. There is a critical power level, typically at the 1 μW level, for the onset of the splitting process. Even so, the splitting signal is not discernible from the BLS data until the input power is much higher, as in the (b) graph of Fig. 2. As elaborated below, these product magnons for the splitting process have a range of frequencies distributed around $f_p/2$. It is important to keep in mind that the wave vector selective BLS measurements are limited to k values below about 3.6×10^4 rad/cm, so that the data do not include the really high k $f_p/2$ magnons. The discussion related to Fig. 3 below will elucidate on this point.

The growth in the peak at f_c [item (3)] is ascribed to the confluence of some subset of these split magnons. In line with the comment above about high k $f_p/2$ magnons, one can

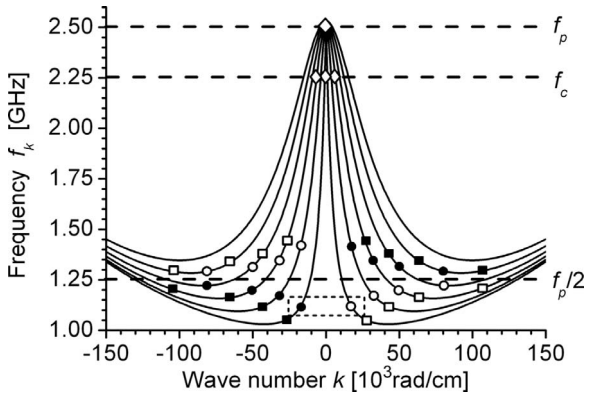

FIG. 3. Schematic dispersion curves of spin-wave frequency f_k vs wave number k with mode connections. The curves are for the first six dipole-exchange spin-wave branches for in-plane propagation parallel or antiparallel to the field H and an H value of 352 Oe, the same as for the data in Fig. 2. The horizontal dashed lines label the frequencies for the three peaks identified in Fig. 2 for the directly pumped magnetostatic backward volume wave spin waves at f_p=2.5 GHz, confluence magnons at f_c, and splitting magnons at $f_p/2$. The open diamond at f_p labels the MSBVW operating point. The matching pairs of solid and open circles and squares show, in schematic form, parametrically excited split magnons at $\pm k$ and with f_k values equally shifted up and down from the $f_p/2$ line. The open diamonds for a range of low $|k|$ values on the f_c line show the nominal position in frequency and wave number for the confluence magnons. The dashed square close to 1.12 GHz identifies split magnons that give a confluence magnon at f_c.

note that there are many options for different confluence frequencies, some above, some below, and some right on top of f_p. This will also become more evident from the Fig. 3 discussion below. This means, among other things that some of the growth noted for the f_p peak with power may be due to f_c type processes. The concluding discussion for this section, given below, provides qualitative connections between these data and the proposed magnon splitting and confluence processes. Quantitative connections will follow in Sec. IV, based on detailed wave vector selective measurements.

These connections are based on the schematic MSBVW spin-wave dispersion diagrams and specific spin-wave mode points shown in Fig. 3. A detailed description of the nomenclature is given in the expanded figure caption. The curves were computed from the standard DESW theory in Ref. 16, standard YIG parameters, and the same film thickness and static field cited for the measurements. The identified mode points are intended to make qualitative connections with the BLS results.

Note that the actual parametric modes need not have wave vectors that are strictly colinear with the field. Keep in mind that a given MSBVW pumped magnon at f_p and wave vector $\mathbf{k}_p$ will split into two parametric magnons with frequencies f_{s1} and f_{s2} and wave vectors $\mathbf{k}_{s1}$ and $\mathbf{k}_{s2}$, respectively. Energy and momentum conservation impose the conditions $f_p=f_{s1}+f_{s2}$ and $\mathbf{k}_p=\mathbf{k}_{s1}+\mathbf{k}_{s2}$. Since $|\mathbf{k}_p|$ is very small compared to $|\mathbf{k}_{s1}|$ and $|\mathbf{k}_{s1}|$, it is clear that $\mathbf{k}_{s1}$ and $\mathbf{k}_{s2}$ must be nearly equal and oppositely directed. The dispersion curve constraints also force both $\mathbf{k}_{s1}$ and $\mathbf{k}_{s2}$ to be nearly colinear with the field. Similar remarks apply to the reverse confluence process that take various pairs of split magnons into modes at frequencies close to f_c. The up shift in frequency to $f_k \approx f_c$ in this case leads to allowed modes at relatively large propagation angles. As the data of Sec. IV will show, the parametric spin waves turn out to have in-plane propagation angles away from the field direction by $\pm 10°$ or so for the split $f_p/2$ magnons and by $\pm 45°$ or so for the confluence f_c magnons.

Overall, Fig. 3 shows a consistent map of the connections between the initially excited cw MSBVW spin-wave signal in the YIG strip and the parametric magnons observed from the BLS measurements. If one considers a low wave-number MSBVW mode at f_p (upper open diamond), magnon splitting processes that conserve frequency and momentum give product magnons as indicated by the square and circle points clustered around the $f_p/2$ line cut in the figure. At the same time, the lower frequency subset of these split magnons can be combined to give a confluence peak at f_c. The dashed box in the lower central part of Fig. 3 identifies two such modes.

The layout of modes in Fig. 3 leads to one more important connection with the data. Note that both the splitting peak in Fig. 2 at $f_p/2$ and the confluence peak at f_c are rather broad. Based on the scenario given above, one can explain the $f_p/2$ line broadening in terms of the relatively wide band of split magnons shown by the circle and square points in Fig. 3. It also stands to reason that if the observed split magnon peak is broad, any peak due to the confluence of these magnons will also be broad.

Taken at face value, the connections implied in Fig. 3 are nothing more than conjecture. The mode connections are based entirely on the dispersion curves shown and the frequencies match those found in the experiment. What remains is to show, from actual wave vector selective BLS data, that the split modes clustered around $f_p/2$ in frequency and the product low wave-number confluence modes at f_c match the data.

IV. WAVE VECTOR SELECTIVE ANALYSIS

The techniques and procedures for the wave vector selective BLS analysis were outlined in Sec. II. Recall that there are two stages in the analysis for the split magnons, one with a variable diameter diaphragm for wave-number analysis and one with a rotating slit aperture for wave vector direction analysis. Recall the key feature of the stage one measurements, namely, the clear and distinct $f_p/2$ peak in Fig. 2(d) that appears suddenly when the diameter of the wave vector selective aperture is larger than about 9 mm. This critical d value corresponds to $k_{\max} \approx 1.1 \times 10^4$ rad/cm. This is precisely the minimum allowed k value for $f_p/2$ magnons from DESW theory. This match-up comprises prima face evidence for the connection with DESW magnons as proposed above.

Figure 4 shows representative wave vector selective BLS data for the $f_p/2$ peak in Fig. 2 and companion isofrequency magnon wave vector contour plots for the low order DESW spin-wave dispersion branches at $f_k=f_p/2$. Graph (a) shows the BLS signal as a function of the cutoff $k_{\max}$ wave-number value. The vertical dashed lines denote the upper and lower limit $k_{\max}$ values for the diaphragm setup described above. Figure 4(b) shows calculated isofrequency contour plots for

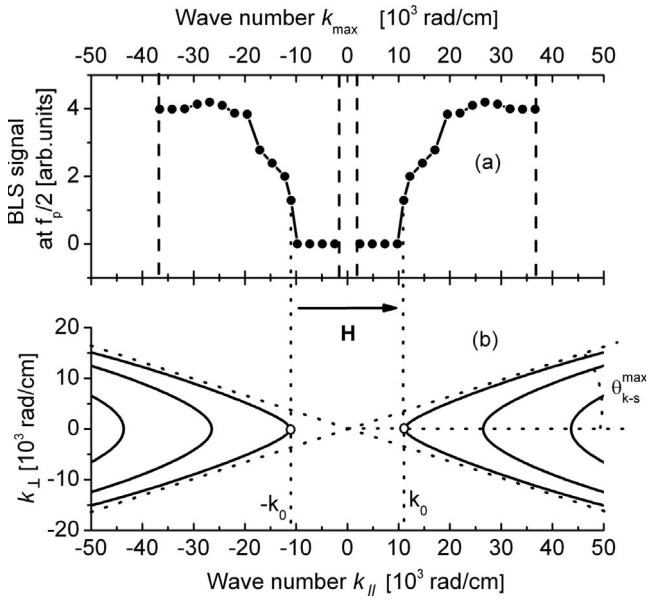

FIG. 4. (a) BLS scattering signal at $f_p/2$ as a function of the maximum allowed wave number k_{max} for an input power of 5.56 mW and f_p=2.5 GHz. The vertical dashed lines denote the limit k_{max} values for the experimental diaphragm setup. (b) Theoretical isofrequency contour plots of the transverse in-plane spin-wave wave vector component $k_\perp$ vs the parallel component $k_\parallel$ for the three lowest-order DESW modes at $f_p/2$. The plot was obtained from the DESW theory of Ref. 16, with parameters that match the experiment. The open circles and k_0 labels mark the low limit for the available DESW spin waves at $f_p/2$. The angle θ^{max}_{k-s} labeled in (b) shows the maximum allowed spin-wave propagation angle.

the 1.25 GHz cut of the dipole-exchange spin-wave dispersion surface. While the horizontal axes for both graphs correspond to wave number, the plotted parameter in (b) corresponds to the component of the in-plane DESW wave vector **k** that is parallel to the static field **H**, labeled as $k_\parallel$. For comparison purposes, the horizontal scales for (a) and (b) are the same. The vertical scale in (b) corresponds to the in-plane transverse component of **k**, labeled as $k_\perp$. For reference purposes for the discussion of the angle data to follow, the θ^{max}_{k-s} labeled in (b) indicates the maximum theoretical in-plane spin-wave propagation angle for the half-frequency spin waves.

The data in (a) and the isofrequency contours in (b) confirm the match up noted in the introduction to this section. The onset of detected spin waves as a function of the experimental k_{max} value occurs precisely at the theoretical lower limit k value at $k_0 \approx 1.1\times10^4$ rad/cm for the half-frequency DESW spin waves. These lower limit k values are marked in (b) by open circles. Note that this onset point in (b) is for a DESW propagation direction that is parallel to the static field and with a propagation angle θ_k equal to zero or 180° only. The full isofrequency contours in (b), however, provide much more information that the confirmation of this onset point for split magnons. The contours allow one to read off the allowed propagation angles for the split magnons with $k > k_0 = 1.1\times10^4$ rad/cm. From these plots, one expects that the angle selective BLS data will reveal spin-wave propagation angles for the half-frequency spin waves in the range

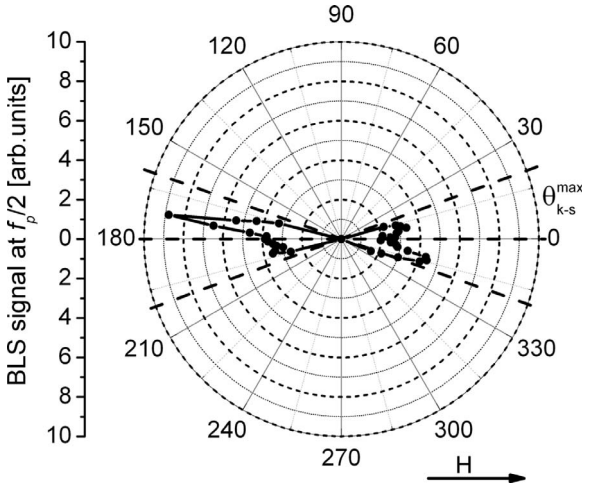

FIG. 5. Polar representation of the BLS signal for the $f_p/2$ DESW magnon peak as a function of the slit aperture rotation angle θ_k. The arrow shows the direction of the static field H. The dashed lines denote the double sector of spin-wave propagation angles for $-\theta^{max}_{k-s} < \theta_k < \theta^{max}_{k-s}$ and $(180°-\theta^{max}_{k-s}) < \theta_k < (180°+\theta^{max}_{k-s})$ that match the range of allowed θ_k values from Fig. 4(b).

$-\theta^{max}_{k-s} < \theta_k < \theta^{max}_{k-s}$ and $(180°-\theta^{max}_{k-s}) < \theta_k < (180°+\theta^{max}_{k-s})$.

As noted previously, θ_k resolved BLS data were obtained with a rotating slit-type aperture scheme. In order to resolve the full 0–360° range of possible θ_k values, the measurements were done with a half-slit arrangement that extends outward from the optical axis in one direction only, rather than the full slit shown in Fig. 1. Figure 5 shows a representative polar plot of BLS intensity data as a function of θ_k for the $f_p/2$ split magnon peak in Fig. 2(d) at P_{in}=5.56 mW. As in Fig. 4, the field is parallel to the θ_k=0 direction. The data were obtained for angular steps of 2° and with the same scanning times for all measurements. The dashed lines at angles of θ^{max}_{k-s} to the horizontal mark the expected range of pumped magnons from Fig. 4. The angular distribution of the DESW $f_p/2$ magnons is clear from the figure and no extensive discussion is needed here. The data show, rather unambiguously, that the BLS signal is constrained within a double sector of angles within $\pm\theta^{max}_{k-s}$ of the field axis. The span of observed propagation angles matches nicely to the contour plot in Fig. 4(b).

The above data and theoretical connections provide a complete map of the DESW $f_p/2$ magnons that result from the three wave splitting process for pumped MSBVW magnons. Both the directly measured wave numbers and the propagation directions of the split magnons match nicely to theory. This represents the first direct experimental map of three magnon splitting processes in any magnetic system pumped in the backward wave configuration.

Turn now to the confluence magnons. Recall that in this case, blocking circles as well as diaphragms and slit apertures were used for the wave vector selective measurements. The changes in intensity with diaphragm diameter d for the f_c peak are quite different from those for the split magnons. In this case, the signal increases steadily as d is increased from 1 to 6 mm and then appears to increase at a slightly lower rate up to the limit d value of 10 mm. This implies that

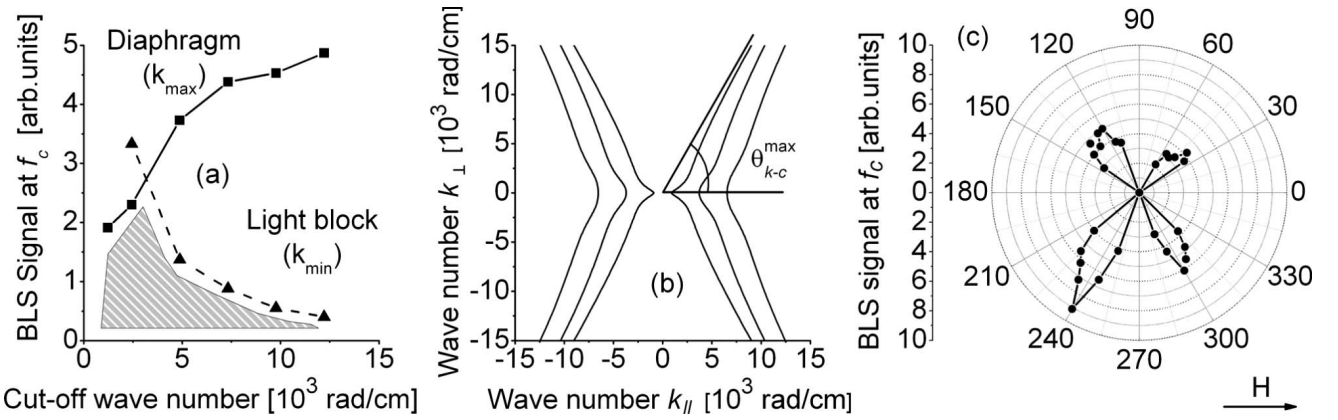

FIG. 6. (a) Data on the BLS scattering signal level at the f_c peak vs the two limit wave numbers $k_{\min}$ and $k_{\max}$, as obtained for different diameter light blocks or diaphragms, respectively. The dashed light gray area gives a qualitative estimate of the confluence magnon k distribution implied by these data. (b) Theoretical isofrequency contour plots of the transverse in-plane spin-wave wave vector component $k_\perp$ vs the parallel component $k_\parallel$, as referenced to the field direction, for the three lowest-order DESW modes at f_c. The plot was obtained from the DESW theory of Ref. 16, with parameters that match the experiment. The angle $\theta_{k-c}^{\max}$ corresponds to the maximum allowed spin-wave propagation angle for confluence magnons at the f_c frequency cut. (c) Polar representation of the BLS signal level at the f_c peak as a function of the slit aperture rotation angle for the input power of 5.56 mW. The arrow shows the direction of the static magnetic bias field **H**.

the predominant confluence magnon k values are generally below about 10^4 rad/cm or so. For the light block in place of the diaphragm, the f_c peak signal intensity starts high and gradually diminishes to near zero as d is increased from the initial 2 mm value to the 10 mm upper limit value. This serves to confirm a confluence magnon distribution with $k < 10^4$ rad/cm and predominant k values somewhat below this limit. At the same time, the slit aperture data indicate propagation angles that are typically $30°-60°$ and $120°-150°$ away from the field axis. Recall that the split magnons are all very close to the field axis. It is clear from these results that the wave vector makeup of the confluence magnons is very different from that for the split magnons.

Figure 6 shows representative wave vector selective BLS data for the f_c peak in Fig. 2 and companion isofrequency magnon wave vector contour plots for the low order DESW spin-wave dispersion branches at $f_k = f_c$. Graph (a) shows the f_c peak intensity as a function of the diaphragm and light block cutoff wave numbers, $k_{\max}$ and $k_{\min}$, as indicated. The shaded curve at the bottom of the graph provides a qualitative indication of the f_c magnon k distribution implied by the two sets of data. Graph (b) shows calculated isofrequency contour plots for the 2.25 GHz f_c cut of the dipole-exchange spin-wave dispersion surface. The angle $\theta_{k-c}^{\max}$ indicates the maximum theoretical in-plane spin-wave propagation angle for the confluence magnons. Graph (c) shows representative BLS data in a polar plot representation for the f_c confluence magnon peak in Fig. 2. In order to obtain the somewhat balanced four-lobe plots shown in (c), it was necessary to use both anti-Stokes positive frequency side BLS data for $90° < \theta_k < 270°$ and Stokes negative frequency side data for $-90°\,(270°) < \theta_k < 90°$.

The results in Fig. 6 provide a useful map of the magnon makeup for the BLS confluence peak. These results also demonstrate the marked difference between these confluence magnons at f_c and the split magnons at $f_p/2$ discussed at the start of this section. Graph (a), for example, shows that the f_c magnons are limited to k values below 10^4 rad/cm, while the data in Fig. 4 show that the split magnons are all at wave numbers well in excess of 10^4 rad/cm. Graph (b) shows, moreover, that the expected angular distribution of the f_c magnons emphasizes propagation directions at about 45° or so, relative to the field axis, while the predominant θ_k values for the split magnons are much closer to the field axis. The angular data in (c) confirm that the magnons associated with the f_c peak do, in fact, give polar plot lobes that match the theory.

V. PUMPING FREQUENCY DEPENDENCES

The results in Secs. III and IV serve to quantify the presence of (1) DESW $f_p/2$ magnons that result from the parametric three wave splitting process for pumped MSBVW magnons, and (2) confluence magnons at f_c that result from the recombination of the DESW magnons. The wave-number makeup and propagation characteristics of these magnons were mapped experimentally and connected to theory. All of these results, however, are based on data for one fixed value of the in-plane field and one specific drive frequency selected for strong coupling to the pumped MSBVW mode. This section is concerned with one further test of the mode connections established above, based on the effect of changes in the pumping frequency f_p on the BLS response, with the field held at the same value as before. The strategy here is similar to that of Synogach *et al.* in Ref. 1. In that work, done for the case of pumped magnetostatic surface modes, an *increase* in both the field and the pumping frequency resulted in an upward shift in both the spin-wave band and the operating point frequency to the point where three magnon splitting processes are no longer allowed. This elimination of three magnon splitting processes resulted in a major change in the microwave response of the surface wave delay line structure.

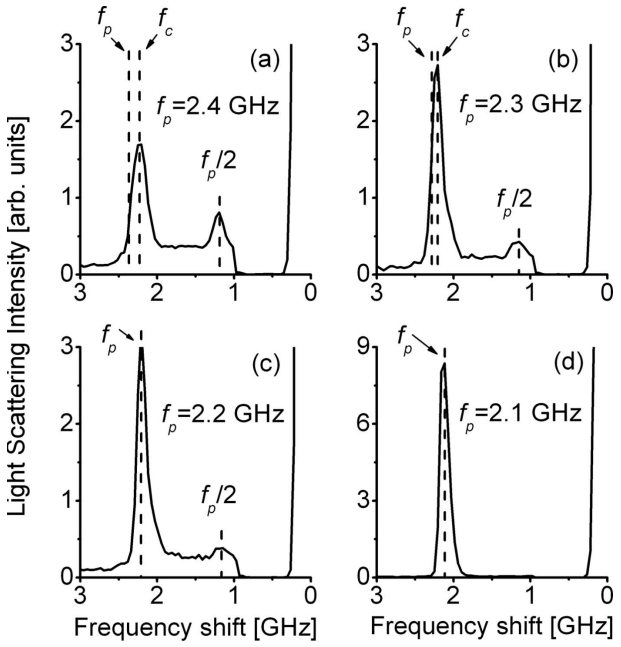

FIG. 7. Representative BLS spectra of scattering intensity vs frequency for different pumping frequencies. (a) f_p=2.4 GHz, (b) f_p=2.3 GHz, (c) f_p=2.2 GHz, and (d) f_p=2.1 GHz. The static external field was set to 352 Oe. The nominal spectrometer free spectral range was 8 GHz. There were no wave vector selective diaphragms or light blocks in place and the measuring time was the same for all scans. The vertical dashed lines and labels identify different peaks in the spectra at f_p, at f_c, and at $f_p/2$.

The approach here is much simpler. The field was held at the same value as before, but now, the pumping frequency was gradually *decreased* to the point where the downshifted $f_p/2$ cut across the spin-wave dispersion curve diagram falls below the bottom of the band of DESW modes. One can see this basic effect from Fig. 3. The bottom of the band sits at about 1.0125 GHz. This means that a pumping frequency below about twice this value, or 2.025 GHz, will be low enough to eliminate the possibility of any three magnon splitting response at all. One can also see that as the pumping frequency is gradually lowered, the $f_p/2$ cut of modes across the bottom of the band will become narrower and narrower and the mean k value for the split magnons will shift out to about 4×10^4 rad/cm just before the splitting response vanishes. This will also cause the f_c point for the confluence magnons to move closer and closer to f_p.

Panels (a)–(d) in Fig. 7 show the effect of a lowering of the pump frequency on the spectra in Fig. 2. The data go from the range where three magnon splitting is readily allowed, as in (a) for f_p=2.4 GHz, to a range where such processes are barely allowed, as in (d) for f_p=2.1 GHz. All data were obtained for the same configuration and parameters as for the data in Fig. 2(d), except for the shift in pumping frequency. The three vertical dashed lines in (a) and (b) mark the pumping frequency operating point (f_p), the confluence (f_c) and splitting ($f_p/2$) peaks from the data, as indicated. In (c), the two vertical dashed lines mark the f_p and $f_p/2$ points only. In this case, the f_c point is so close to the operating point that the two frequencies are indistinguishable. The single vertical dashed line in (d) marks the f_p point only. The vertical axis BLS intensity scales for the four graphs while shown as "arbitrary units" [arb. units] actually show self-consistent relative values. The matching scales for (a), (b), and (c) demonstrate the evolution of the spectra and the individual intensities with the drop in frequency. The larger range for (d) shows the rapid rise in the strength of the f_p peak as one approaches the cutoff point for splitting.

The four panels in Fig. 7 demonstrate the evolution scenario outlined above. Recall that as f_p is gradually reduced, the gap between the $f_p/2$ and the bottom of the band becomes smaller and smaller. This means that the f_c point must also move closer and closer to f_p. This is precisely what one sees from panels (a)–(c) in Fig. 7. For (a) the f_p to f_c spacing has dropped from the nominal 0.25 GHz value in Fig. 2 to 0.1 GHz. For (b) this spacing has dropped further to about 0.05 GHz. In (c), the f_c peak position is not even discernible from f_p on the scale of the graph. Finally, for the case shown in Fig. 7(d), with the bottom of the band at about 1.02 GHz and $f_p/2$ at 1.05 GHz, the half-frequency point is so close to the bottom of the band that the splitting and confluence effects of interest here no longer occur. In panel (d), one sees that the $f_p/2$ splitting peak has disappeared entirely and the peak at f_p has increased in intensity by a factor of 3 or so.

The above points mainly relate to the evolution in the shape of the spectra as the pumping frequency is decreased. Note also that the data show a clear degradation in the shape of the $f_p/2$ splitting peak as one goes from panel (a) to panel (c). This degradation can be attributed, quite plausibly, to two things, (1) the move of the $f_p/2$ frequency cut closer and closer to the bottom of the band, and (2) the wave-number limits in the collection optics. From Fig. 3, one can see that as one moves from the situation shown to a pump frequency at the bottom of the band, the k values for the split frequency modes that contribute to the confluence will move from the indicated value of about 2×10^4 out to about 4×10^4 rad/cm. At the same time, the maximum k value that can be accessed by the collection lens is about 3.6×10^4 rad/cm. This means that the somewhat washed out $f_p/2$ peaks in (b) and (c) are for wave numbers that approach or exceed the limits of the setup.

VI. SUMMARY AND CONCLUSION

Three magnon splitting and confluence processes in thin YIG films for the MSBVW propagation configuration has been experimentally observed by Brillouin light scattering measurements and confirmed by wave vector selective analysis. A complete characterization for both of these nonlinear processes has been made. The change in the response with pumping frequency as well as the fully analyzed wave vector makeup of the product magnons provides proof positive of these processes. Interestingly, and perhaps fortuitously, the data reveal a confluence response for only selected half-frequency split magnons that are slightly downshifted from the strict half-frequency point. This state of affairs pushes the confluence peak to a point slightly below the peak at the signal frequency and renders it observable.

ACKNOWLEDGMENTS

This work was supported in part by the United States Army Research Office, MURI, Grant No. W911NF-04-1-0247, the United States Office of Naval Research, Grants No. N00014-07-1-0597 and No. N00014-08-1-1050 (through sub-Award No. PT103701-SC101157 from Virginia Commonwealth University), and the Russian Foundation for Basic Research, Grant No. 08-02-00959. Ward L. Johnson, National Institute of Standards and Technology, Boulder, Colorado, is acknowledged for a perceptive reading of the paper.

[1] V. T. Synogach, Yuri K. Fetisov, C. Mathiue and C. E. Patton, Phys. Rev. Lett. **85**, 2184 (2000).
[2] C. Mathieu, V. T. Synogach, and C. E. Patton, Phys. Rev. B **67**, 104402 (2003).
[3] H. Suhl, J. Phys. Chem. Solids **1**, 209 (1957).
[4] J. W. Boyle, S. A. Nikitov, A. D. Boardman, J. G. Booth, and K. Booth, Phys. Rev. B **53**, 12173 (1996).
[5] M. Bauer, C. Mathieu, S. O. Demokritov, B. Hillebrands, P. A. Kolodin, S. Sure, H. Dötsch, V. Grimalsky, Yu. Rapoport, and A. N. Slavin, Phys. Rev. B **56**, R8483 (1997).
[6] H. Xia, P. Kabos, H. Y. Zhang, P. A. Kolodin, and C. E. Patton, Phys. Rev. Lett. **81**, 449 (1998).
[7] O. Büttner, M. Bauer, A. Rueff, S. O. Demokritov, B. Hillebrands, A. N. Slavin, M. P. Kostylev, and B. A. Kalinikos, Ultrasonics **38**, 443 (2000).
[8] N. G. Kovshikov, B. A. Kalinikos, C. E. Patton, E. S. Wright, and J. M. Nash, Phys. Rev. B **54**, 15210 (1996).
[9] V. E. Demidov and N. G. Kovshikov, Tech. Phys. Lett. **24**, 274 (1998); **24**, 647 (1998).
[10] M. Wu, B. A. Kalinikos, and C. E. Patton, Phys. Rev. Lett. **95**, 237202 (2005).
[11] G. Srinivasan and C. E. Patton, IEEE Trans. Magn. **21**, 1797 (1985).
[12] G. Srinivasan, C. E. Patton, and P. R. Emtage, J. Appl. Phys. **61**, 2318 (1987).
[13] W. Wettling, W. D. Wilber, P. Kabos, and C. E. Patton, Phys. Rev. Lett. **51**, 1680 (1983).
[14] W. D. Wilber, W. Wettling, P. Kabos, C. E. Patton, and W. Jantz, J. Appl. Phys. **55**, 2533 (1984).
[15] W. D. Wilber, J. G. Booth, C. E. Patton, G. Srinivasan, and R. W. Cross, J. Appl. Phys. **64**, 5477 (1988).
[16] B. A. Kalinikos, Sov. Phys. J. **24**, 718 (1981).